

BRIEF COMMUNICATION OPEN

Large-area borophene sheets on sacrificial Cu(111) films promoted by recrystallization from subsurface boron

Rongting Wu^{1,2}, Adrian Gozar^{1,2} and Ivan Božović^{1,2,3}

Borophene, an atomically thin covalently bonded boron sheet, has attracted great attention as a novel quantum material because of its structural tunability and potential utilization in flexible and transparent electronics. So far, borophene has been synthesized on silver or copper single crystals, but these substrates are small, very expensive, and unsuitable for study of transport properties or electronics applications. Here, we report synthesis of borophene on nanometer-scale thick Cu(111) films grown on sapphire. We have developed a process of enlarging faceted borophene islands, by repeated submersion of boron into copper at high temperature and resurfacing and re-crystallization at lower temperature. This discovery was enabled by real-time feedback from low-energy electron microscopy and diffraction. We demonstrate synthesis of borophene as faceted micrometer-size monocrystal islands or as full-monolayer sheets. The process is scalable to wafer size; moreover, Cu films could be sacrificed and sapphire reused. Our work opens the door for new experiments and brings applications one step closer.

npj Quantum Materials (2019)4:40; <https://doi.org/10.1038/s41535-019-0181-0>

INTRODUCTION

Synthesis of atomically thin covalently bonded materials such as silicene,^{1,2} germanene,^{3,4} stanene^{5,6} etc., have greatly enriched the two-dimensional (2D) materials family. Their extraordinary physical properties could be utilized in the next generation electronics, photonics, and clean energy technologies. The recent synthesis of 2D boron sheets, borophene, has attracted much interest due to its unique anisotropic flexibility and metallicity, and also because of the unprecedented diversity of structures arising from complex bonding patterns and atomic-scale geometries. Initial theoretical predictions of polymorphism of free-standing 2D boron sheets,^{7–10} as well as tunability of the structure by the choice of the substrate,^{11,12} distinguish borophene as a promising platform for discovery of novel materials with tunable physical properties.

As the lightest elemental 2D network, borophene is a promising candidate for phonon-mediated superconductivity. In MgB₂, 2D atomic boron planes isostructural to graphene already stand out by sustaining superconductivity with a high critical temperature ($T_c = 39$ K). Recent theoretical calculations predict $T_c \approx 10$ –20 K for borophene with different hexagonal vacancy patterns.^{13–15} In view of the intrinsic polymorphism, structural anisotropy, and inherent metallic conductivity, borophene is also a candidate for applications in photonic and plasmonic devices¹⁶ because of the large frequency range of its plasmonic response.

Despite the considerable interest in 2D boron sheets, the experimental synthesis of borophene trailed its prediction by more than 10 years. This was a great challenge because the 3D bulk counterpart, (which does not have a naturally layered structure), is lower in energy than any of the flat polymorphs.^{17,18} In order to surmount this thermodynamic disadvantage, substrates with sufficient adhesion to boron atoms have been suggested for the synthesis of 2D boron.^{11,12} Recently, Mannix et al.¹⁹ and Feng et al.²⁰ reported successful synthesis of

atomically thin 2D boron islands, tens of nanometers in size, grown on Ag(111) substrates using molecular beam epitaxy (MBE) under ultrahigh vacuum (UHV) conditions. Two borophene phases, denoted as β_{12} and χ_3 with the hexagonal vacancy ratios $\eta = 1/6$ and $\eta = 1/5$, respectively, were synthesized. These pioneering studies have stimulated many subsequent experimental and theoretical studies. Signatures of metallic bands²¹ and Dirac fermions^{22,23} in borophene on Ag(111) have been observed in angle-resolved photoemission spectroscopy (ARPES). Demonstration of borophene-based heterostructures²⁴ and atomic-level understanding of borophene line defects²⁵ indicate a potential pathway for its implementation in nanoelectronics and devices.

Notwithstanding these promises for unique electronic, mechanical, and photonic properties, the nanoscale borophene islands grown on Ag(111) are far too small for device fabrication. This hinders the study of key transport properties such as resistivity, Hall effect and magnetoresistance, since micrometer-size single-crystal flakes are needed for such measurements. In a recent study,²⁶ we addressed this challenge by growing borophene on single-crystal Cu(111) substrates and monitoring the synthesis process by low-energy electron microscopy (LEEM). A new borophene phase was discovered and single-crystal domains 100 μm^2 in size produced.²⁶

Cu substrates have been commonly used for the chemical vapor deposition (CVD) growth of high-quality large-area single-crystal graphene. Graphene has also been successfully grown on Cu buffer films deposited on sapphire.^{27,28} This Cu buffer were subsequently 'sacrificed' by dissolving it in FeCl₃ solution, leaving a free-standing graphene film that then can be repositioned on any supporting substrate of choice; moreover, sapphire substrates were reused multiple times.²⁹ Our objective was to achieve similar results with borophene, and this is the main result of this work.

¹Department of Applied Physics, Yale University, New Haven, CT 06520, USA; ²Energy Sciences Institute, Yale University, West Haven, CT 06516, USA and ³Brookhaven National Laboratory, Upton, NY 11973, USA

Correspondence: Ivan Božović (bozovic@bnl.gov)

Received: 1 April 2019 Accepted: 16 July 2019

Published online: 02 August 2019

Using LEEM to monitor the films in real-time under UHV conditions, we have established a procedure to fabricate high-quality single-crystal Cu(111) films by post-annealing an as-deposited amorphous copper film on sapphire. The film quality was evaluated and verified by in-situ low-energy electron diffraction (LEED) and by ex-situ X-ray diffraction (XRD). Then, again enabled by real-time LEEM and LEED observations, we have discovered a new procedure to synthesize large-area single-crystal borophene on the single-crystal Cu(111) films. Large-area faceted borophene islands can be produced, or the entire substrate can be covered with a single-monolayer borophene film. Important for conceived electronics applications, this process is scalable; sapphire is readily available commercially in 12-inch wafer size. Removing Cu while supporting borophene by a non-conducting substrate would enable accurate measurement of its intrinsic transport properties.

RESULTS

Single-crystals of Cu(111) films growth on $\text{Al}_2\text{O}_3(0001)$

High-quality Cu(111) films are synthesized by secondary-grain growth method:^{30–32} an amorphous copper film is first grown on sapphire and then crystallized in-situ by post annealing at elevated temperature. The nucleation and growth of such a Cu (111) film are illustrated in Fig. 1, which shows several snapshots of bright-field LEEM images taken at different temperatures. More details can be seen in Supplementary Video 1. The crystalline Cu (111) phase is colored reddish-brown while the amorphous copper area is depicted as gray. A pure-copper source (a custom-designed Knudsen-cell evaporator) was directed at the heated $\text{Al}_2\text{O}_3(0001)$ substrate and used to deposit a 50–100 nm thick amorphous copper film. Figure 1a shows the typical bright-field LEEM image taken directly after copper film deposition with the $\text{Al}_2\text{O}_3(0001)$ substrate kept at $T_s = 513$ K. The field of view is $6\ \mu\text{m}$ wide. In as-deposited film, almost the entire surface is occupied by amorphous copper, but some irregularly shaped crystal nuclei (reddish-brown color) with the lateral size on the scale of tens to hundreds of nanometers can be seen as well. We have found that for the best results it is important to keep a fairly low substrate temperature, $T_s \approx 510$ K during copper film

deposition; copper films grown at T_s higher than about 600 K typically show rough surfaces with large and multi-oriented crystal nuclei.

In-situ crystallization of copper film was initiated by slowly increasing the substrate temperature and monitored in real-time by bright-field LEEM. In Fig. 1b–h, we show snapshots of copper film morphology at different temperatures. The field of view is $20\ \mu\text{m}$. The initial annealing process at $T_s \approx 700$ –800 K causes the crystalline copper islands to grow larger while their density decreases; the amorphous copper area shrinks concomitantly. As shown in Fig. 1b, after annealing at $T_s = 794$ K, we see the formation of micrometer-sized crystalline copper islands with straight boundaries, highlighted in Fig. 1b–e by green arrows. Notably, the surfaces of these islands are not atomically flat as can be discerned by the contrast variation on the reddish copper islands.

With further annealing at the temperature in the 800–1060 K range, the lateral extent of crystallized copper islands keeps increasing and the coalescence process is activated. As shown in Fig. 1e, at $T_s = 1057$ K most of the crystallized copper islands are large, have flat surfaces and faceted shapes, and in total cover about 50% of the surface. Furthermore, as highlighted by white dashed lines, some straight boundaries with relative angles of 60° or 120° appear, indicating that the crystallized copper islands may assume the $\langle 111 \rangle$ orientation. Upon increasing the substrate temperature further to $T_s = 1070$ K, we found the lateral extent of crystallized islands to increase dramatically. Eventually, crystalline copper film with continuous and curved step edges, as well as micrometer-sized terraces cover the whole surface, see Fig. 1f–h.

We found that the optimal temperature for annealing amorphous copper films varies depending on the film thickness. Typically, thicker copper films can endure annealing at higher temperatures and/or for longer time. De-wetting of the copper film can happen if it is annealed at too high temperature for too long time. Using LEEM to monitor the crystallization process in real-time, we can stop annealing as soon as the high-quality Cu (111) crystal film is formed (Supplementary Video 1) and prevent copper de-wetting.

The crystallography of the crystallized copper films was further studied by XRD using $\text{Cu-K}\alpha$ radiation in the θ - 2θ geometry, within the range $20^\circ < 2\theta < 85^\circ$, which covers the main peaks of a

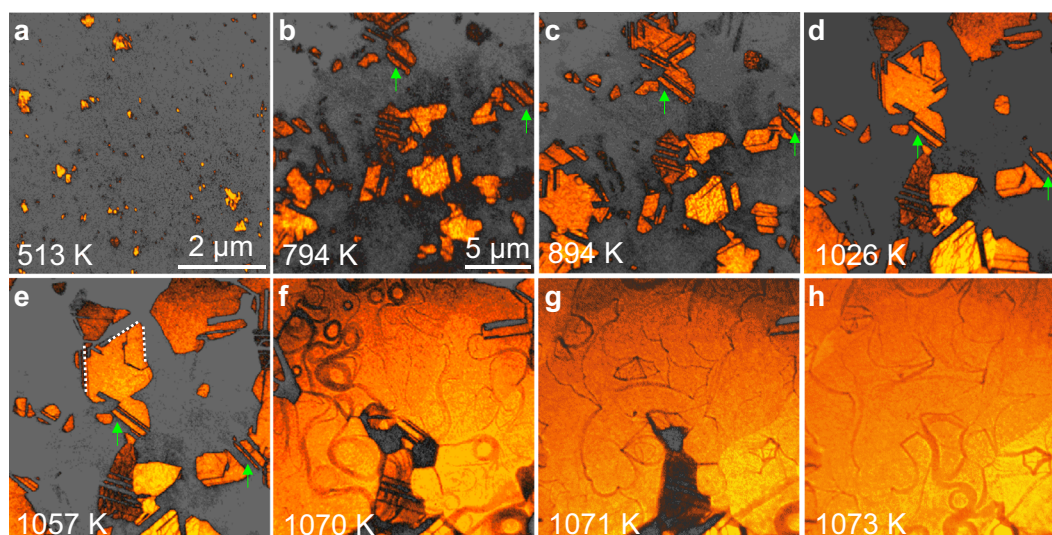


Fig. 1 Real space LEEM images of Cu(111) film crystallization process on $\text{Al}_2\text{O}_3(0001)$ surface. **a** Bright-field LEEM images taken after copper film deposition on $\text{Al}_2\text{O}_3(0001)$ surface at $T_s = 513$ K. The field of view is $6\ \mu\text{m}$. The amorphous copper film is tinted gray and the Cu crystal nuclei as reddish-brown. **b–h** Bright-field LEEM images taken successively during the post-annealing of Cu film at different temperatures as indicated. The field of view is $20\ \mu\text{m}$. The Cu(111) crystal islands (tinted reddish brown) slowly grow and eventually cover the whole surface. The detailed dynamics of crystallization process is shown in Supplementary Video 1

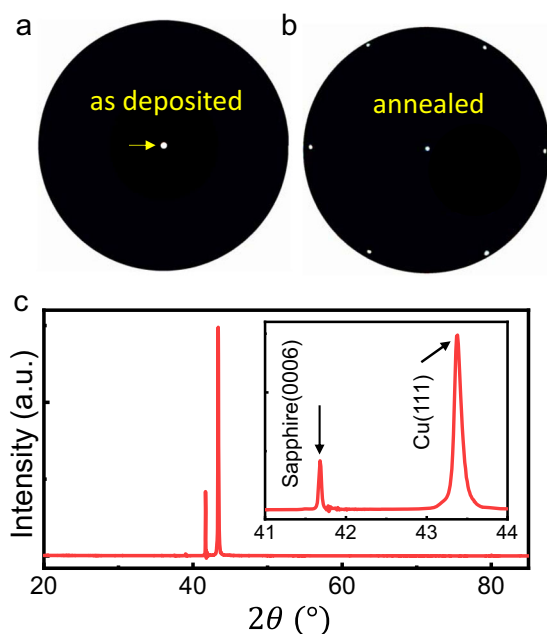


Fig. 2 Diffraction from copper film on sapphire, as deposited and after post-annealing. **a** Typical LEED pattern taken at room temperature on the copper film deposited on $\text{Al}_2\text{O}_3(0001)$ surface at $T_s = 513$ K. The specular (00) reflection spot is indicated by the yellow arrow. The energy of electrons was 24 eV. The contribution from inelastic electron scattering has been filtered out. **b** A typical LEED pattern from a post-annealed Cu film, recorded at room temperature. Apart from the central (00) spot, six very sharp spots appear, corresponding to Bragg diffraction from Cu(111) surface. The energy of electrons was 45 eV. **c** XRD data from a post-annealed Cu(111) crystal film on $\text{Al}_2\text{O}_3(0001)$ surface. The two pronounced peaks from Cu(111) and sapphire together with the clean background testify to the high film quality

face-centered cubic structure. The XRD pattern shown in Fig. 2c features two strong peaks (indicated by the black arrows in the inset), one at $2\theta = 41.68^\circ$ and the other at $2\theta = 43.38^\circ$, corresponding to the diffraction from the $\text{Al}_2\text{O}_3(0006)$ and the Cu(111) planes, respectively. Apart from the Cu(111) and $\text{Al}_2\text{O}_3(0006)$ peaks, no other Bragg reflections are detected.³³ Together with our in-situ LEED data, this indicates that an epitaxial Cu(111) film has formed on the sapphire surface after the high-temperature annealing.

Full-monolayer borophene synthesis on crystal Cu(111) film on sapphire

In Fig. 3, we show a sequence of bright-field LEEM images illustrating the nucleation and growth process of a borophene sheet that eventually covers the whole Cu(111) crystal film on sapphire. The dynamics of the growth is shown in more detail in Supplementary Video 2. Here, the substrate temperature was $T_s = 760$ K and the growth rate was 0.08 ML/min (Supplementary Video 2). For better contrast, borophene crystals are tinted blue, while the Cu(111) surface is colored yellow-reddish brown. Figure 3a depicts the surface morphology of the Cu(111) crystal film before borophene growth. The smooth step edges indicate the high quality of the surface. As the boron atoms are deposited onto the surface, they accumulate at the step edges and form the initial borophene nuclei, as seen in Fig. 3b, c. With further boron deposition, the density of the borophene crystal nuclei increases up to the maximum of around $4.6 \mu\text{m}^{-2}$. Past that, the borophene islands steadily grow in size. While most of the borophene islands display irregular shapes, one can identify some well-faceted islands, as highlighted by the green lines in Fig. 3c–e. As even

more boron atoms are deposited, all the borophene islands grow and merge together until eventually a full monolayer is formed, as shown in Fig. 3h. A typical LEED pattern taken from this full monolayer borophene sheet is shown exhibited in Fig. 3i. It agrees very well with previously reported²⁶ LEED patterns of borophene grown on Cu(111) bulk crystals, showing a superposition of all six domains.

The self-limiting growth of borophene on bulk Cu(111) substrate²⁶ was also observed here. Beyond one-full-monolayer coverage, the growth rate of borophene film decreases dramatically. This is auspicious since it enables the synthesis of uniform, atomically thin borophene sheets on Cu(111) crystal buffers on sapphire.

Faceted borophene islands synthesis

Beside the full monolayer borophene growth on Cu(111) crystal film, large-area faceted monodomain borophene islands are also of great interest as a promising platform to study the anisotropic material physics and electron scattering at borophene island boundaries. The successful growth of large-area faceted borophene islands is demonstrated in Fig. 4. Figure 4a presents an enlargement of the bright-field LEEM image shown in Fig. 3c. It is clear that most borophene islands here are quite small, irregularly shaped, and densely distributed on the surface. This mainly results from dense step edges and defects on the underlying Cu(111) crystal film surface.

Taking advantage of the in-situ real-time monitoring capability of LEEM technique, we have studied in detail the process of borophene dissolution into the bulk of Cu at high temperature and its resurfacing and re-crystallization on Cu(111) surface²⁶ during cool-down. Armed with this knowledge, we succeeded in synthesizing large-area faceted borophene islands on a Cu(111) crystal film. The recipe includes several cycles of high temperature ($T_s \approx 900$ K) annealing of the borophene flakes densely packed as shown in Fig. 4a and re-growing borophene at $T_s = 760$ K assisted by additional boron deposition. In this way, we successfully synthesize micrometer-sized, triangle-shaped borophene monocrystal islands as shown in Fig. 4b. It is clear that for a comparable coverage, the borophene flakes in Fig. 4b are much larger than those in Fig. 4a. The density of crystal nuclei decreases to around $1.4 \mu\text{m}^{-2}$, which is comparable to that on a bulk-crystal Cu(111) substrate.²⁶ The borophene structure is confirmed by additional LEED pattern (Fig. 4c) taken on re-crystallized triangle borophene islands in Fig. 4b, with atomic structure model shown in Fig. 4d. Furthermore, most borophene islands are triangle-shaped and share the same orientation, as highlighted by the green-dashed triangles. This, indeed, opens the prospects for interesting new device-physics experiments.

DISCUSSION

The synthesis of large-area high quality borophene sheet on thin Cu(111) film on sapphire opens the possibility of transferring borophene to insulating substrates, by sacrificing the Cu(111) buffer. Compared to a bulk single-crystal Cu(111) substrate, a thin film offers the advantages of lower cost and shorter etching time. Note that sacrificial thin Cu(111) films on sapphire have been already utilized for graphene. That process employed the conventional chemical vapor deposition (CVD) technique for graphene synthesis^{27,28} on top of a thin Cu(111) buffer film. After graphene growth, the Cu buffer is dissolved and graphene is transferred to a more suitable substrate.^{34,35} The connection between these well-established techniques and the large-scale high-quality borophene sheet synthesis on crystal Cu(111) film thus sets the stage for promising borophene transfer and device fabrication.

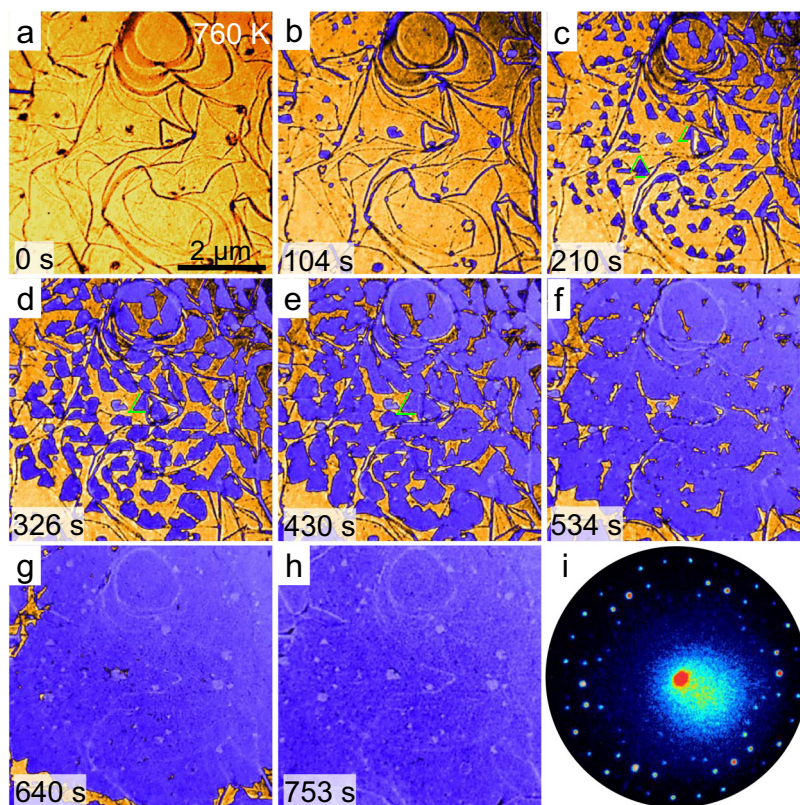


Fig. 3 Growth of borophene on Cu(111) crystal film on sapphire. **a–h** Bright-field LEEM images recorded at different times during borophene growth at $T_s = 760$ K on the surface of a Cu(111) crystal film deposited on an $\text{Al}_2\text{O}_3(0001)$ substrate as described in Fig. 1. The field of view is $6 \mu\text{m}$. The clean Cu(111) surface, with the step edges clearly visible, is tinted by reddish-brown color. Borophene single-crystal islands, tinted by blue color, slowly grow until they cover the entire surface. The film growth rate was 0.08 monolayers of borophene per minute. **i** A typical LEED pattern taken after borophene growth on Cu(111) crystal film. This pattern originates from a superposition of all six rotational domains. The energy of electrons was 15 eV

Potentially interesting phenomena may be hosted by borophene-graphene heterostructures. To avoid potential chemical contamination and/or degradation of borophene during solution-based transfer, one may be able to utilize some recently developed techniques such as encapsulated delamination transfer³⁶ used in silicene device fabrication. The programmed vacuum stack (PVS) process³⁷ for layer-by-layer 2D materials assembly may be pertinent as well.

The Cu(111) films with nanoscale thickness used here for the large-area borophene synthesis are also superior to bulk single-crystal Cu(111) substrates insofar that the films screen AC electromagnetic fields very weakly, thus making possible contactless AC-susceptibility measurements. Mutual inductance^{38–43} measurements could be carried out in order to probe whether the 2D boron sheets can sustain superconductivity and determine the critical temperature (T_c) and London penetration depth (λ_L).

To conclude, we report the successful growth of high-quality sacrificial Cu(111) crystal film on sapphire and subsequent large-area, high-quality borophene synthesis on top under UHV conditions. Crystalline Cu(111) film was grown by physical vapor deposition of copper atoms on sapphire surface at a fairly low substrate temperature ($T_s = 510$ K) and subsequently annealed at a high temperature. The film morphology was monitored by LEEM in real time, and the crystal orientation was determined by in-situ LEED and ex-situ by XRD. The dynamics of the subsequent synthesis of borophene on top of Cu(111) film was studied by LEEM in real time, from the clean Cu(111) surface up to full borophene monolayer coverage. By multi-cycles of high-temperature ($T_s \approx 900$ K) annealing and borophene re-growing at $T_s = 760$ K, we also synthesized well oriented, micrometer-sized,

triangle-shaped borophene islands. The capability to synthesize large-area high-quality borophene sheet on sacrificial crystal Cu(111) film on sapphire demonstrated in this work sets the stage for future borophene transfer and device fabrications to explore its promising electronic and optical properties.

METHODS

Synthesis of Cu(111) film on sapphire

Single-crystal $\alpha\text{-Al}_2\text{O}_3(0001)$ substrates were degassed at $T_s = 1370$ K for 1 h in an UHV chamber with base pressure $p = 2 \times 10^{-10}$ Torr. Then, the substrate temperature was lowered to $T_s = 510$ K for copper film deposition. Copper was evaporated from a custom-designed Knudsen-cell source kept at $T_{\text{Cu}} = 1320$ K. The resulting Cu film was amorphous as expected and verified by the absence of Bragg diffraction spots in LEED. Post-annealing of the as deposited amorphous copper films on sapphire was carried out at $700 \text{ K} < T_s < 1100$ K. The film growth and post-annealing processes were monitored in real-time using an Elmitec LEEM-III system augmented with molecular beam epitaxy capability. Annealing was carried out until the crystal Cu(111) phase covers the whole surface, and large and flat terraces form on the Cu surface. Typically, thicker copper films require a higher post-annealing temperature and/or a longer annealing time to fully crystallize. Real-time LEEM monitoring enables us to quickly find the optimal temperature and stop annealing in time before dewetting happens.

The annealed copper films were cooled down to room temperature, with the crystal quality analyzed in-situ by LEED. Subsequently, XRD data were taken ex-situ using a Rigaku Smart Lab X-ray Diffractometer equipped with a Cu K_α source (the X-ray wavelength of 1.5406 \AA).

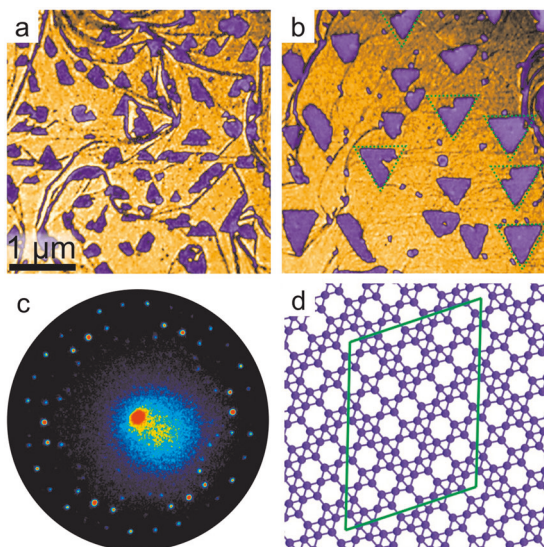


Fig. 4 Synthesis of large-area, faceted borophene islands on Cu film on sapphire. **a** As-grown borophene islands on Cu(111) films, at half-coverage, are typically quite small and irregularly shaped. **b** Borophene islands at similar coverage but with larger lateral extent and faceted shapes. This was achieved by several cycles of high-temperature annealing to dissolve boron into the copper film and cooling down for borophene to re-grow. Real-time monitoring by LEEM was used to determine the optimal annealing temperatures and times for formation of large-area faceted islands. The field of view is $4\ \mu\text{m}$ for both images. **c** A typical LEED pattern taken on recrystallized borophene shown in the panel **b**. This pattern originates from a superposition of all six rotational domains. The energy of electrons was 15 eV. **d** Atomic structure of borophene on Cu(111) film on sapphire. The green rhomboid indicates the unit cell corresponding to the LEED data

Synthesis of borophene on Cu(111) film

The growth of borophene on crystal Cu(111) film was performed in the same UHV LEEM/MBE system. The process was essentially the same as the one we developed for borophene growth on bulk-crystal Cu(111) substrates.²⁶ The base pressure of the UHV chamber is $p = 2 \times 10^{-10}$ Torr. Boron atoms were evaporated from an electron-beam source with a heating power of 30–50 W. The electron beam was focused on a pure boron rod (ESPI, purity >99.9999%) 3 mm in diameter. The substrate temperature was kept at $T_s = 760$ K during borophene growth. Micrometer-size, triangle-shaped borophene islands were synthesized by several cycles of post-annealing of initially irregular borophene islands at $T_s = 900$ K and borophene re-growing at $T_s = 760$ K. Real-time monitoring of in-situ borophene growth by LEEM together with precise control of boron deposition enable synthesis of high-quality borophene with desired coverage.

DATA AVAILABILITY

All data needed to evaluate the conclusions in this paper are included in the paper. Additional data related to this paper may be requested from I.B. (bozovic@bnl.gov).

ACKNOWLEDGEMENTS

R.W. and A.G. were supported by the Gordon and Betty Moore Foundation's EPIQS Initiative through Grant GBMF4410. I.B. was supported by the US Department of Energy, Basic Energy Sciences, Materials Sciences, and Engineering Division. The ex-situ XRD measurements were supported by Yale West Campus Materials Characterization Core (MCC).

AUTHOR CONTRIBUTIONS

R.W. performed the film synthesis and characterization. I.B. proposed and supervised the project. All authors contributed to the paper.

ADDITIONAL INFORMATION

Supplementary information accompanies the paper on the *npj Quantum Materials* website (<https://doi.org/10.1038/s41535-019-0181-0>).

Competing interests: The authors declare no competing interests.

Publisher's note: Springer Nature remains neutral with regard to jurisdictional claims in published maps and institutional affiliations.

REFERENCES

- Meng, L. et al. Buckled silicene formation on Ir(111). *Nano Lett.* **13**, 685–690 (2013).
- Feng, B. J. et al. Evidence of silicene in honeycomb structures of silicon on Ag (111). *Nano Lett.* **12**, 3507–3511 (2012).
- Li, L. F. et al. Buckled germanene formation on Pt(111). *Adv. Mater.* **26**, 4820–4824 (2014).
- Dávila, M. E. et al. Germanene: a novel two-dimensional germanium allotrope akin to graphene and silicene. *New J. Phys.* **16**, 095002 (2014).
- Zhu, F.-f. et al. Epitaxial growth of two-dimensional stanene. *Nat. Mater.* **14**, 1020–1025 (2015).
- Deng, J. et al. Epitaxial growth of ultraflat stanene with topological band inversion. *Nat. Mater.* **17**, 1081–1086 (2018).
- Tang, H. & Ismail-Beigi, S. Novel precursors for boron nanotubes: the competition of two-center and three-center bonding in boron sheets. *Phys. Rev. Lett.* **99**, 115501 (2007).
- Yang, X., Ding, Y. & Ni, J. Ab initio prediction of stable boron sheets and boron nanotubes: structure, stability, and electronic properties. *Phys. Rev. B* **77**, 041402 (2008).
- Tang, H. & Ismail-Beigi, S. Self-doping in boron sheets from first principles: a route to structural design of metal boride nanostructures. *Phys. Rev. B* **80**, 134113 (2009).
- Penev, E. S., Bhowmick, S., Sadrzadeh, A. & Yakobson, B. I. Polymorphism of two-dimensional boron. *Nano Lett.* **12**, 2441–2445 (2012).
- Liu, Y., Penev, E. S. & Yakobson, B. I. Probing the synthesis of two-dimensional boron by first-principles computations. *Angew. Chem.* **125**, 3238–3241 (2013).
- Zhang, Z., Yang, Y., Gao, G. & Yakobson, B. I. Two-dimensional boron monolayers mediated by metal substrates. *Angew. Chem. Int. Ed.* **54**, 13022–13026 (2015).
- Penev, E. S., Kutana, A. & Yakobson, B. I. Can two-dimensional boron superconduct? *Nano Lett.* **16**, 2522–2526 (2016).
- Zhao, Y., Zeng, S. & Ni, J. Superconductivity in two-dimensional boron allotropes. *Phys. Rev. B* **93**, 014502 (2016).
- Gao, M., Li, Q.-Z., Yan, X.-W. & Wang, J. Prediction of phonon-mediated superconductivity in borophene. *Phys. Rev. B* **95**, 024505 (2017).
- Huang, Y., Shirodkar, S. N. & Yakobson, B. I. Two-dimensional boron polymorphs for visible range plasmonics: a first-principles exploration. *J. Am. Chem. Soc.* **139**, 17181–17185 (2017).
- Zhang, Z., Penev, E. S. & Yakobson, B. I. Polyphony in B flat. *Nat. Chem.* **8**, 525–527 (2016).
- Sun, X. et al. Two-dimensional boron crystals: structural stability, tunable properties, fabrications and applications. *Adv. Funct. Mater.* **27**, 1603300 (2017).
- Mannix, A. J. et al. Synthesis of borophenes: anisotropic, two-dimensional boron polymorphs. *Science* **350**, 1513–1516 (2015).
- Feng, B. et al. Experimental realization of two-dimensional boron sheets. *Nat. Chem.* **8**, 563–568 (2016).
- Feng, B. et al. Direct evidence of metallic bands in a monolayer boron sheet. *Phys. Rev. B* **94**, 041408 (2016).
- Feng, B. et al. Dirac fermions in borophene. *Phys. Rev. Lett.* **118**, 096401 (2017).
- Feng, B. et al. Discovery of 2D anisotropic dirac cones. *Adv. Mater.* **30**, 1704025 (2017).
- Liu, X. et al. Self-assembly of electronically abrupt borophene/organic lateral heterostructures. *Sci. Adv.* **3**, e1602356 (2017).
- Liu, X. et al. Intermixing and periodic self-assembly of borophene line defects. *Nat. Mater.* **17**, 783–788 (2018).
- Wu, R. et al. Large-area single-crystal sheets of borophene on Cu(111) surfaces. *Nat. Nanotech.* **14**, 44–49 (2019).
- Verguts, K. et al. Epitaxial $\text{Al}_2\text{O}_3(0001)/\text{Cu}(111)$ template development for CVD graphene growth. *J. Phys. Chem. C* **120**, 297–304 (2016).
- Reddy, K. M. et al. High quality, transferrable graphene grown on single crystal Cu (111) thin films on basal-plane sapphire. *Appl. Phys. Lett.* **98**, 113117 (2011).
- Nagai, Y. et al. Ten-second epitaxy of Cu on repeatedly used sapphire for practical production of high-quality graphene. *ACS Omega* **2**, 3354–3362 (2017).
- Thompson, C. V. Secondary grain growth in thin films of semiconductors: theoretical aspects. *J. Appl. Phys.* **58**, 763–772 (1985).

31. Thompson, C. V., Frost, H. J. & Spaepen, F. The relative rates of secondary and normal grain growth. *Acta Metall.* **35**, 887–890 (1987).
32. Miller, D. L. et al. Giant secondary grain growth in Cu films on sapphire. *AIP Adv.* **3**, 082105 (2013).
33. Janssen, G. C. A. M. & Kwakernaak, C. Comment on “High quality, transferrable graphene grown on single crystal Cu(111) thin films on basal-plane sapphire” [Appl. Phys. Lett. 98, 113117 (2011)]. *Appl. Phys. Lett.* **99**, 086101 (2011).
34. Suk, J. W. et al. Transfer of CVD-grown monolayer graphene onto arbitrary substrates. *ACS Nano* **5**, 6916–6924 (2011).
35. Caldwell, J. D. et al. Technique for the dry transfer of epitaxial graphene onto arbitrary substrates. *ACS Nano* **4**, 1108–1114 (2010).
36. Tao, L. et al. Silicene field-effect transistors operating at room temperature. *Nat. Nanotech.* **10**, 227–231 (2015).
37. Kang, K. et al. Layer-by-layer assembly of two-dimensional materials into wafer-scale heterostructures. *Nature* **550**, 229–233 (2017).
38. Fiory, A. T., Hebard, A. F., Mankiewich, P. M. & Howard, R. E. Penetration depths of high T_c films measured by two-coil mutual inductances. *Appl. Phys. Lett.* **52**, 2165–2167 (1988).
39. Claassen, J. H., Reeves, M. E. & Soulen, R. J. Jr. A contactless method for measurement of the critical current density and critical temperature of superconducting rings. *Rev. Sci. Instrum.* **62**, 996–1004 (1991).
40. Turneaure, S. J., Pesetski, A. A. & Lemberger, T. R. Numerical modeling and experimental considerations for a two-coil apparatus to measure the complex conductivity of superconducting films. *J. Appl. Phys.* **83**, 4334–4343 (1998).
41. Božović, I., He, X., Wu, J. & Bollinger, A. T. Dependence of the critical temperature in overdoped copper oxides on superfluid density. *Nature* **536**, 309–311 (2016).
42. He, X., Gozar, A., Sundling, R. & Božović, I. High-precision measurement of magnetic penetration depth in superconducting films. *Rev. Sci. Instrum.* **87**, 113903 (2016).
43. Duan, M.-C. et al. Development of in situ two-coil mutual inductance technique in a multifunctional scanning tunneling microscope. *Rev. Sci. Instrum.* **88**, 073902 (2017).



Open Access This article is licensed under a Creative Commons Attribution 4.0 International License, which permits use, sharing, adaptation, distribution and reproduction in any medium or format, as long as you give appropriate credit to the original author(s) and the source, provide a link to the Creative Commons license, and indicate if changes were made. The images or other third party material in this article are included in the article's Creative Commons license, unless indicated otherwise in a credit line to the material. If material is not included in the article's Creative Commons license and your intended use is not permitted by statutory regulation or exceeds the permitted use, you will need to obtain permission directly from the copyright holder. To view a copy of this license, visit <http://creativecommons.org/licenses/by/4.0/>.

© The Author(s) 2019